Turbulent Boundary Layers on Surfaces Covered With Filamentous Algae

Michael P. Schultz
Department of Mechanical Engineering,
United States Naval Academy,
Annapolis, MD 21402

Turbulent boundary layer measurements have been made on surfaces covered with filamentous marine algae. These experiments were conducted in a closed return water tunnel using a two-component, laser Doppler velocimeter (LDV). The mean velocity profiles and parameters, as well as the axial and wall-normal turbulence intensities and Reynolds shear stress, are compared with flows over smooth and sandgrain rough walls. Significant increases in the skin friction coefficient for the algae-covered surfaces were measured. The boundary layer and integral thickness length scales were also increased. The results indicate that profiles of the turbulence quantities for the smooth and sandgrain rough walls collapse when friction velocity and boundary layer thickness are used as normalizing parameters. The algae-covered surfaces, however, exhibited a significant increase in the wall-normal turbulence intensity and the Reynolds shear stress, with only a modest increase in the axial turbulence intensity. The peak in the Reynolds shear stress profiles for the algae surfaces corresponded to the maximum extent of outward movement of the algae filaments. [S0098-2202(00)01902-7]

Introduction

Biofouling is the colonization of a surface exposed in the aquatic environment by microorganisms, plants, and animals. On marine vehicles, biofouling leads to increased surface roughness and frictional drag. In the past, calcareous or ''hard'' fouling organisms such as barnacles were the most problematic to ship operators. At present, the duty cycles of modern merchant ships, marked by short periods in port and in larvae-rich coastal areas, favor the settlement and growth of algae (Callow [1]). The most common macroalgae found on copper-based antifouling paints is the filamentous green alga *Enteromorpha*. Its dominance results from its nearly global distribution, high reproductive potential, and ability to withstand large variations in environmental conditions (Callow [2]). Since filamentous algae can form a significant presence on the hulls of marine vehicles, their effect on skin friction and turbulent boundary layer structure is of practical interest.

A substantial body of research has been devoted to studying the effects of marine fouling on frictional resistance. A review of much of this work was given in Schultz [3]. Atmospheric boundary layer investigations over plant canopies are analogous in many respects, and a review of this work is given in Raupach and Thom [4] and Raupach et al. [5]. Several studies have looked at the effect of flexible vegetation on turbulent shear flows and, therefore, are of particular relevance to the present investigation. Kouwen and Unny [6] studied turbulent open channel flow over plastic strips. The primary contribution of their work was the formulation of a dimensionless, stiffness parameter that related the density and amount of bending stress of the roughness to the wall shear stress. The stiffness parameter proposed by Kouwen and Unny was as follows:

$$\frac{1}{k_0}\left(\frac{mEI}{\rho U_\tau^2}\right)^{1/4} \tag{1}$$

Lewkowicz and Das [7] used uniformly distributed nylon tufts attached to a rough flat plate to model a turbulent boundary layer flow over a filamentous algae layer. Both mean and turbulence quantities were measured. They found that the model algae layer caused significant increases in the physical growth of the boundary layer, the wall shear stress, and the turbulent normal and shear stresses. The roughness function, ΔU^+, for their model algae film collapsed well to Eq. (2) for $40 \leqslant k^+ \leqslant 800$.

$$\Delta U^+ = \frac{0.89}{\kappa}\ln(k^+) + 1.055 \tag{2}$$

Ikeda et al. [8] used both laser Doppler velocimetry (LDV) and particle image velocimetry (PIV) to study the organized, three-dimensional vortical motions above flexible aquatic plants. The plants were modeled using nylon filaments. They noted that the mean axial velocity profile had an inflection point below the top of the roughness layer. The turbulent normal and shear stresses were found to be largest near the top of the roughness layer. The wavy motion often associated with flow over filamentous surfaces (e.g., the waves in a field of grain) was shown to be induced by the movement of elliptical vortices generated intermittently above the vegetation layer.

Schultz and Swain [9] investigated the effect of natural, algal biofilms on turbulent boundary layers. The roughness layers tested were composed mainly of diatom slimes and blue-green algae, with only one specimen having a significant coverage of filamentous macroalgae. The results showed an increase in C_f of 33 percent to 187 percent on the fouled specimens. The biofilms tested showed varying effect on the turbulent normal and shear stresses when those quantities were normalized with the friction velocity. It was concluded that a large part of the variability in the results was due to the heterogeneity of the biofilms that were tested.

The aim of the present experimental investigation was to better understand the structure of turbulent boundary layers that develop over natural, filamentous marine algae layers. To accomplish this, boundary layer measurements were made on test surfaces colonized by algae. The experiments were conducted in water tunnel using a two-component LDV. The mean velocity profiles and bulk flow parameters as well as the turbulent normal and shear stresses are compared with flows over smooth and sandgrain rough walls.

Experimental Facilities and Method

The experimental work was carried out at the Harbor Branch Oceanographic Institution (HBOI) closed return, closed jet water

Contributed by the Fluids Engineering Division for publication in the JOURNAL OF FLUIDS ENGINEERING. Manuscript received by the Fluids Engineering Division October 20, 1999; revised manuscript received February 8, 2000. Associate Technical Editor: J. K. Eaton.

Downloaded 01 Apr 2008 to 131.122.81.5. Redistribution subject to ASME license or copyright; see http://www.asme.org/terms/Terms_Use.cfm

tunnel (Gangadharan et al. [10]). The tunnel is 2.44 m in height, 8.53 m in length, and 1.22 m in width, and the test section is 0.61 m by 0.61 m and is 2.54 m in length. Flow management devices include turning vanes placed in the tunnel corners and a polycarbonate honeycomb flow straightener in the entrance to the contraction section. The resulting freestream turbulence intensity in the test section is ~1.3 percent.

The test matrix consisted of five specimens. One smooth surface and specimens covered with #240 grit and #36 grit sandpaper served as controls. The remaining two specimens were allowed to foul with the filamentous green alga, *Enteromorpha spp.* over a period of about 30 days. In order to look at boundary layer development over the algae layer, velocity profiles were taken at five downstream positions. These were taken at 1.15 m, 1.30 m, 1.45 m, 1.60 m, and 1.75 m downstream of the leading edge of the test fixture and at a nominal freestream velocity of 1.6 ms^{-1}.

The algae used in the present study were grown at the HBOI Aquaculture facility. Water from the Indian River Lagoon was continuously pumped through a sand filtration system and into grow-out tanks. During the experiments, the salinity of the water in the tanks ranged from 25 ppt to 40 ppt. The water temperature ranged from 25°C to 35°C. Test specimens were fabricated from cast acrylic sheet and were exposed for ~30 days. Each specimen measured 558 mm in width, 1168 mm in length, and 12.7 mm in thickness. Still digital photographs and video clips of the algae layer under flow were taken. Image analysis allowed the mean thickness of the layer to be estimated. This was accomplished by digitizing the side profile of the algae layer and measuring its height above the acrylic substrate. The roughness height of the sandgrain rough specimens was measured using a BMT stylus-type hull roughness analyzer. The stylus was 1.6 mm in diameter and the profile length was 50 mm. The maximum peak to valley height was measured 100 times and averaged to estimate the roughness height for the surface. The accuracy of the device is ±0.01 mm or ±5 percent, whichever is greater. A description of the test surfaces with their roughness heights is given in Table 1.

The test specimens were inserted into a flat plate test fixture mounted horizontally in the tunnel. The plate was 0.58 m in width, 2.06 m in length, and 54 mm thick. It was constructed of polyvinylchloride (PVC) and stainless steel and was mounted horizontally in the tunnel's test section. The leading edge of the test fixture was shaped to mimic the forward portion of a NACA 0012-64 airfoil. The forward most 280 mm of it was covered with #36 grit sandpaper to hasten development of a turbulent boundary layer. The use of a strip of roughness to artificially thicken a boundary layer was proposed by Klebanoff and Diehl [11]. The forward edge of the specimen was located 710 mm from the leading edge of the plate.

Velocity measurements were made using a TSI two-component, fiber-optic LDV system. The LDV used a four beam arrangement and was operated in backscatter mode. The probe volume diameter was ~90 μm, and its length was ~1.3 mm. The viscous length (ν/U_τ) varied from a minimum of 9 μm for the algae covered surface to a maximum of 18 μm for the smooth wall. The diameter of the probe volume, therefore, ranged from 10 viscous lengths for the algae covered surface to 5 viscous lengths for the smooth wall. The LDV probe was mounted on an AMPRO System 1618, three-axis traverse unit. The traverse allowed the position of the probe to be maintained to ± 5 μm in all directions. In order to facilitate two-component, near wall measurements, the probe was tilted downwards at an angle of 4 deg to the horizontal and was rotated 45 deg about its axis. Using this setup, measurements were made as close as 50 μm to the wall. Velocity measurements were conducted in coincidence mode with 30,000 random samples per location. Doppler bursts for the two channels were required to fall within a 40 μs coincidence window or the sample was rejected.

In this study, two methods were used to determine the skin friction coefficient, C_f, for each of the test specimens. For the smooth surface, C_f was found using the Clauser chart method with the log-law constants $\kappa=0.41$ and $B=5.0$. The total stress method, as presented in Ligrani and Moffat [12], was used to verify these results. For the rough walls, C_f and ε were obtained using the modified Clauser chart procedure given by Perry and Li [13]. Again, the total stress method was used to verify the C_f values obtained using the modified Clauser chart. The roughness functions for the rough wall profiles were obtained using the law of the wall (Eq. (3)) with the previously obtained values of U_τ and ε.

$$U^+=\frac{1}{\kappa}\ln(y+\varepsilon)^++B-\Delta U^+ \tag{3}$$

The boundary layer thickness and Coles' wake parameter for all of the profiles was then found by using a nonlinear least squares algorithm to fit the experimental data from the overlap region out to ~0.9δ to Coles' law of the wake in universal defect form (Eq. (4)).

$$\frac{U_e-U}{U_\tau}=-\frac{1}{\kappa}\ln\left[\frac{(y+\varepsilon)}{\delta}\right]+\frac{2\Pi}{\kappa}\left[\cos^2\left(\frac{\pi}{2}\frac{(y+\varepsilon)}{\delta}\right)\right] \tag{4}$$

Uncertainty Estimates

Precision uncertainty estimates for the velocity measurements were made using repeatability tests. Ten replicate profiles were taken on both a smooth and a rough plate. The standard error for each of the measurement quantities was then calculated for both samples. In order to estimate the 95 percent confidence limits for a statistic calculated from a single profile, the standard error was multiplied by the two-tailed t value ($t=2.262$) for 9 degrees of freedom and $\alpha=0.05$, as given by Coleman and Steele [14]. The resulting precision uncertainties in the mean velocities were ±0.7 percent in the outer region of the boundary layer and ±1.5 percent in the near-wall region. For $\overline{u'^2}$ and $\overline{v'^2}$, the precision was ±1.4

Table 1 Description of test surfaces

Specimen	k (mm)	St. Dev. (mm)	% Roughness Coverage	Description
Smooth	NA	NA	NA	Cast acrylic surface
#240 grit sandpaper	0.07	0.03	100	#240 grit commercial wet/dry sandpaper
#36 grit sandpaper	0.93	0.11	100	#36 grit commercial wet/dry sandpaper
Algae #1	6.4	1.3	50	filamentous, green algae (*Enteromorpha spp.*) with underlying diatomaceous slime film; individual algae filaments up to 71 mm in length
Algae #2	3.8	0.4	35	filamentous, green algae (*Enteromorpha spp.*) with underlying diatomaceous slime film; individual algae filaments up to 58 mm in length

Downloaded 01 Apr 2008 to 131.122.81.5. Redistribution subject to ASME license or copyright; see http://www.asme.org/terms/Terms_Use.cfm

percent in the outer region and ± 2.7 percent in the near-wall region. The precision uncertainty in $\overline{u'v'}$ was ± 5 percent.

LDV measurements are also susceptible to a variety of bias errors including fringe bias, validation bias, velocity bias, and velocity gradient bias. Fringe bias is due to the fact that scattering particles passing through the measurement volume at large angles may not be measured since several fringe crossing are needed to validate a measurement. In this experiment, the fringe bias was considered insignificant, as the beams were shifted well above the burst frequency representative of twice the freestream velocity (Edwards [15]). Validation bias results from filtering too close to the signal frequency and any processor biases. In general these are difficult to estimate and vary from system to system. No corrections were made to account for validation bias. Velocity bias results from the greater likelihood of high velocity particles moving through the measurement volume during a given sampling period. The present measurements were burst transit time weighted (Buchhave et al. [16]) to correct for velocity bias. Velocity gradient bias is due to variation in velocity across the measurement volume. The correction scheme of Durst et al. [17] was used to correct u'. The corrections to the mean velocity and the other turbulence quantities were quite small and therefore neglected. An additional bias error in the v' measurements of ~ 2 percent was caused by introduction of the w' component due to inclination of the LDV probe.

The uncertainties in C_f for the smooth walls using the Clauser chart and the total stress method were ± 5 percent and ± 7 percent, respectively. The uncertainties in C_f for the rough walls using the modified Clauser chart and the total stress method were ± 10 percent and ± 13 percent, respectively. The increased uncertainty for the rough walls resulted mainly from the extra two degrees of freedom (ε and ΔU^+) in the analysis. The uncertainties in δ, δ^*, and θ were ± 8 percent, ± 5 percent, and ± 6 percent, respectively.

Results and Discussion

The bulk flow parameters for the five test specimens are given in Table 2. The displacement, momentum, and boundary layer thickness for the algae-covered surfaces were all significantly increased with respect to the smooth wall values. The average increases in δ^*, θ, and δ for algae #1 were 81 percent, 57 percent, and 18 percent, respectively. For algae #2, the increases in δ^*, θ, and δ were 83 percent, 58 percent, and 19 percent above the smooth wall values. Results from Lewkowicz and Das [7], on a simulated filamentous algae layer, showed that it increased the boundary layer thickness by 25 percent to 30 percent above that of a background roughness.

In the present study, increases in the mean values of δ^*, θ, and δ were also noted on the sandgrain rough surfaces, although not to as great an extent. Only slight increases in the integral length scales and boundary layer thickness, all of which fell within the uncertainty of the measurements, were noted on the 240-grit surface. Average increases in δ^* and θ of 53 percent and 34 percent, respectively, were found on the 36-grit surface. The boundary layer thickness was also increased slightly on this surface, but the increase was not significant given the uncertainty in the measurement.

Figure 1 presents C_f versus Re_θ for all the test surfaces using the Clauser chart methods. The results of Coles [18] are also shown for comparison. It is of note that good agreement between the Clauser chart (or modified Clauser chart) and the total stress method was seen for most of the profiles. The mean absolute difference in C_f from the two methods was 3 percent for the smooth surface, 4 percent for the sandgrain rough surfaces, and 6 percent for the algae-covered surfaces. The skin friction coefficients for algae #1 averaged 125 percent higher than the smooth wall values, while algae #2 averaged 110 percent higher. The increase in C_f for 36-grit sand roughness averaged 84 percent. The skin friction coefficients for the 240-grit sand roughness were 9 percent higher than the smooth wall, but this is not a significant difference given the experimental uncertainty. It should be noted that the present smooth wall C_f results averaged 3 percent higher than those of Coles [18].

Table 2 Boundary layer parameters

Specimen	x (m)	U_e (ms^{-1})	Re_θ	δ (mm)	δ* (mm)	θ (mm)	H
Smooth	1.15	1.50	4020	28	3.7	2.8	1.35
	1.30	1.53	4400	31	4.0	3.0	1.33
	1.45	1.46	4700	33	4.4	3.4	1.31
	1.60	1.50	5250	36	4.8	3.7	1.32
	1.75	1.53	5570	38	5.0	3.8	1.29
240-grit	1.15	1.56	4870	29	4.2	3.1	1.35
	1.30	1.55	5150	32	4.4	3.3	1.35
	1.45	1.53	5410	33	4.6	3.5	1.34
	1.60	1.56	5730	36	4.8.	3.6	1.33
	1.75	1.56	6130	39	4.9	3.8	1.28
36-grit	1.15	1.60	6510	30	5.5	3.7	1.50
	1.30	1.61	6890	33	6.0	3.9	1.55
	1.45	1.59	8130	35	6.7	4.6	1.48
	1.60	1.60	8850	39	7.4	4.9	1.53
	1.75	1.61	9390	42	7.8	5.3	1.48
Algae #1	1.15	1.61	6400	30	5.4	3.5	1.53
	1.30	1.64	8270	34	7.0	4.5	1.56
	1.45	1.67	9910	40	8.4	5.3	1.58
	1.60	1.66	11700	45	9.2	6.3	1.47
	1.75	1.70	13020	49	10.1	6.8	1.49
Algae #2	1.15	1.56	7270	30	6.1	4.0	1.53
	1.30	1.54	8850	36	7.5	4.9	1.55
	1.45	1.56	9680	40	8.1	5.3	1.54
	1.60	1.59	11070	44	9.0	5.9	1.53
	1.75	1.53	11380	48	9.4	6.3	1.49

Figures 2 and 3 show the mean velocity profiles for algae #1 and #2 as they develop downstream. Included for comparison is Eq. (5), the smooth wall log-law using the Stanford Conference values for the slope and intercept (Coles [19]).

$$U^+ = 5.62 \log y^+ + 5.0 \tag{5}$$

One feature of interest in these graphs is the roughness function. The results of Schultz and Swain [9] showed erratic streamwise variation in ΔU^+ for turbulent boundary layers developing over slime films. The authors attributed this to the heterogeneous

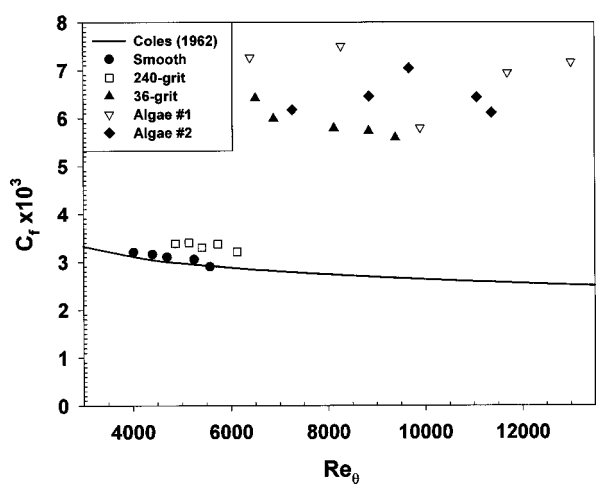

Fig. 1 Skin friction coefficient versus momentum thickness Reynolds number for the five test specimens (uncertainties in C_f: ±5 percent for the smooth specimen; ±10 percent for fouled profiles)

Downloaded 01 Apr 2008 to 131.122.81.5. Redistribution subject to ASME license or copyright; see http://www.asme.org/terms/Terms_Use.cfm

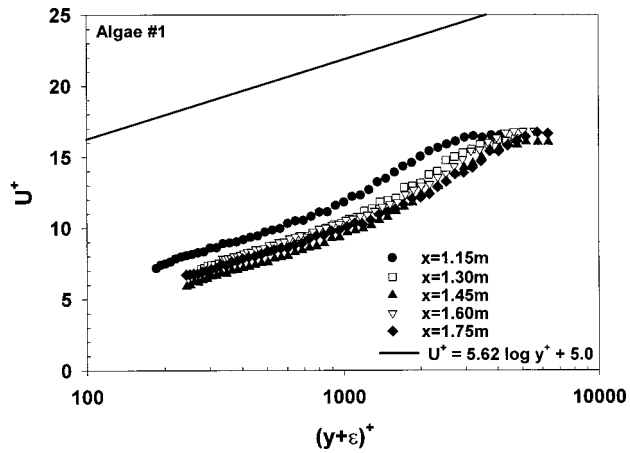

Fig. 2 Mean velocity profiles for algae #1 (uncertainty in U^+ ±7 percent)

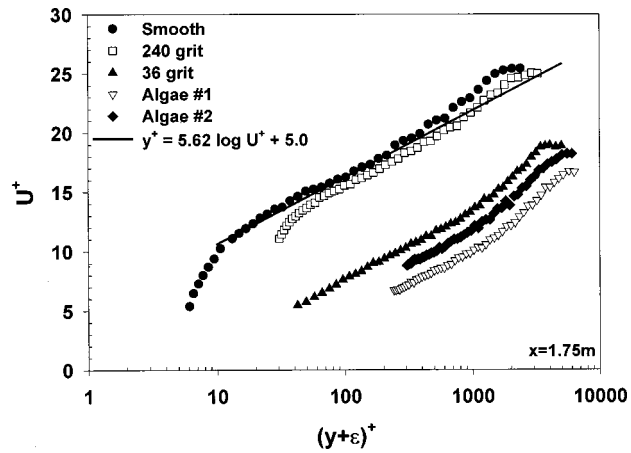

Fig. 4 Mean velocity profiles for the five test specimens @ $x = 1.75$ m (uncertainty in U^+: ±4 percent for the smooth surface; ±7 percent for the rough surfaces)

nature of the biofilms that were tested. The present results were taken on fairly uniform, filamentous algae layers, and the erratic behavior of the roughness function is notably absent. Figure 4 shows the mean velocity profiles for all five test specimens at $x = 1.75$ m. The figure illustrates that the roughness functions for the two algae-covered plates were larger than for the sandgrain rough surfaces.

The roughness functions for the rough test surfaces are presented in Fig. 5. Also included are the roughness functions for uniform sand roughness as given by Colebrook and White [20], Schlichting [21], and Bandyopadhyay [22]. It was not the primary aim of the present investigation to develop relationships that correlate some physical measure of algae to their roughness function. To attempt this would require measurements over a much larger U_τ range than were taken in this study. It is interesting, however, to see how the present results compare those of standard roughness types. The scatter in the values of ΔU^+ versus k^+ was larger for the algae-covered specimens than for the sandgrain rough specimens. This is likely due to nonuniformities in the thickness and composition of the algae surface. The results of Schultz and Swain [9] on highly heterogeneous slime roughness showed significantly more scatter than the present results.

Profiles of the turbulent normal stresses, $\overline{u'^2}/U_\tau^2$ and $\overline{v'^2}/U_\tau^2$, and the turbulent shear stress, $\overline{-u'v'}/U_\tau^2$, for algae #1 are presented in Figs. 6, 7, and 8, respectively. The graphs are shown to illustrate the downstream development in the turbulence quantities

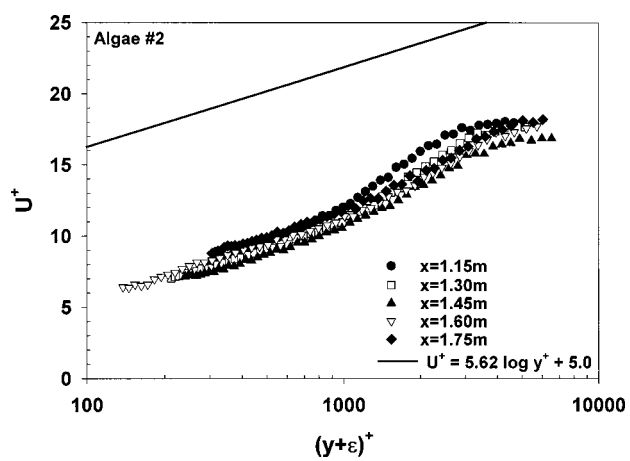

Fig. 3 Mean velocity profiles for algae #2 (uncertainty in U^+ ±7 percent)

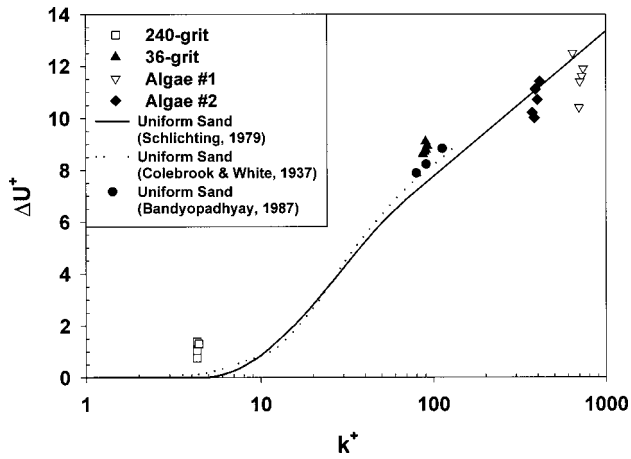

Fig. 5 Roughness functions for the test specimens (uncertainty in ΔU^+ ±13 percent)

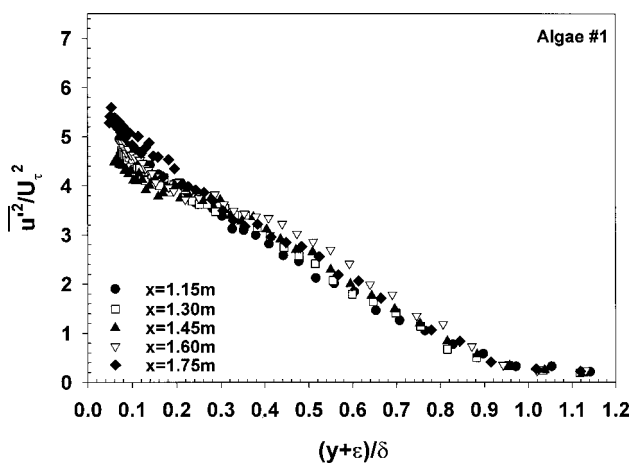

Fig. 6 Turbulent normal stress $\overline{u'^2}/U_\tau^2$ for algae #1 (uncertainty in $\overline{u'^2}/U_\tau^2$ ±10 percent)

over the filamentous algae layer. Similar results were also obtained for algae #2. Although there is some scatter, the results indicate that the turbulence profiles over these algae layers reach a nearly self-similar state.

The profiles of the turbulent normal stress, $\overline{u'^2}/U_\tau^2$, for all the

Downloaded 01 Apr 2008 to 131.122.81.5. Redistribution subject to ASME license or copyright; see http://www.asme.org/terms/Terms_Use.cfm

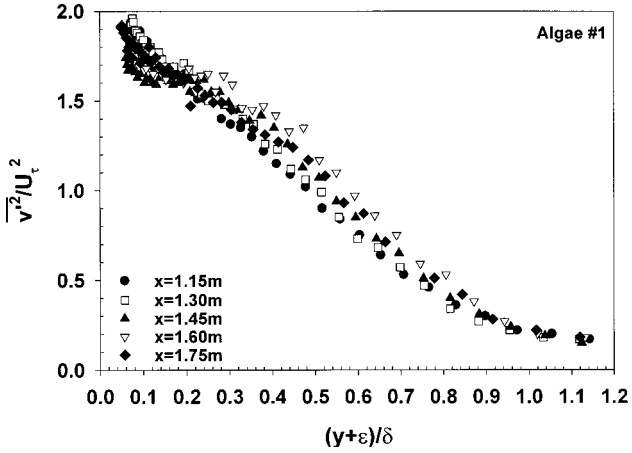

Fig. 7 Turbulent normal stress $\overline{v'^2}/U_\tau^2$ for algae #1 (uncertainty in $\overline{v'^2}/U_\tau^2$ ±10 percent)

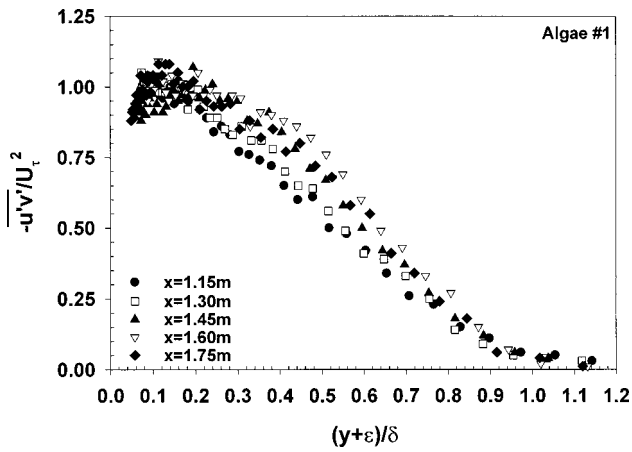

Fig. 8 Turbulent shear stress $-\overline{u'v'}/U_\tau^2$ for algae #1 (uncertainty in $-\overline{u'v'}/U_\tau^2$ ±11 percent)

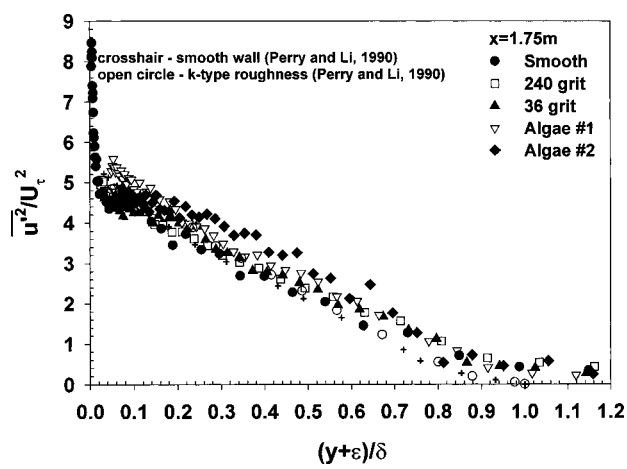

Fig. 9 Turbulent normal stress $\overline{u'^2}/U_\tau^2$ for all the test surfaces @ $x=1.75$ m (uncertainty in $\overline{u'^2}/U_\tau^2$: ±6 percent for the smooth surface; ±10 percent for the rough surfaces)

test surfaces at $x=1.75$ m are shown in Fig. 9. Also included in the graph are the data of Perry and Li [13] for a smooth wall and a *k*-type, mesh roughness. Reasonable agreement between the present results and those of Perry and Li is seen. The exceptions are the algae covered surfaces. Algae #1 showed a modest increase in $\overline{u'^2}/U_\tau^2$ near the roughness layer, and algae #2 exhibited an increase in $\overline{u'^2}/U_\tau^2$ over a larger region of the boundary layer. The present experimental results also agree qualitatively with those of Krogstad et al. [23] who found only a modest change in $\overline{u'^2}/U_\tau^2$ for a mesh-type roughness compared to a smooth wall boundary layer.

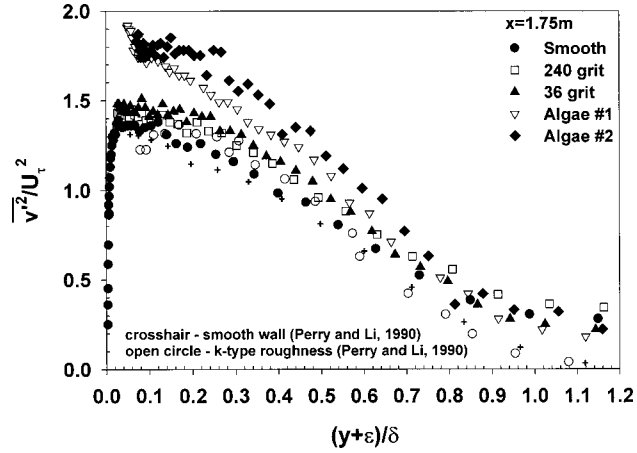

Fig. 10 Turbulent normal stress $\overline{v'^2}/U_\tau^2$ for all the test surfaces @ $x=1.75$ m (uncertainty in $\overline{v'^2}/U_\tau^2$: ±6 percent for the smooth surface; ±10 percent for the rough surfaces)

Profiles of the turbulent normal stress, $\overline{v'^2}/U_\tau^2$, for all the test surfaces at $x=1.75$ m are shown in Fig. 10. The results of Perry and Li [13] are included for comparison. Agreement among the present smooth and sandgrain rough results and those of Perry and Li was seen. Both algae-covered surfaces showed significant increases in $\overline{v'^2}/U_\tau^2$ over both the smooth and sandgrain rough surfaces. The increase amounted to ~ 30 percent near the roughness layer and was observed well out into the outer region of the boundary layer. Image analysis of the video clips of the algae under flow indicates that the maximum extent of outward movement of the filaments during turbulent bursts was $\sim 0.18\delta$ and $\sim 0.15\delta$ for algae #1 and #2, respectively, at $x=1.75$ m. The region of significantly increased $\overline{v'^2}/U_\tau^2$ extends to >2.5 times the maximum extent of outward movement of the filaments. It is of note that Krogstad et al. [23] also observed a significant increase in $\overline{v'^2}/U_\tau^2$ for fully-rough boundary layer flow over mesh roughness. Krogstad and Antonia [24] concluded that the major effect

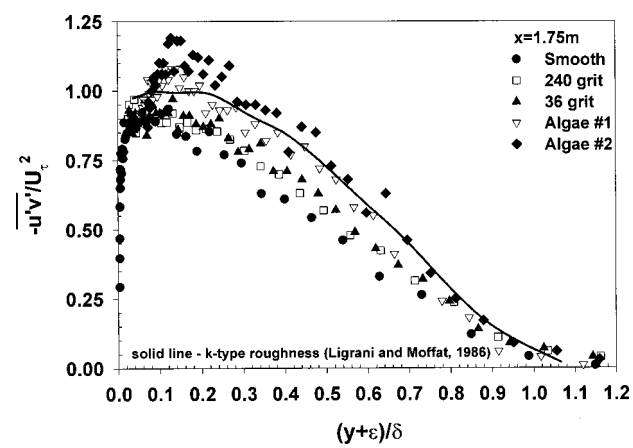

Fig. 11 Turbulent shear stress $-\overline{u'v'}/U_\tau^2$ for all the test surfaces @ $x=1.75$ m (uncertainty in $-\overline{u'v'}/U_\tau^2$: ±7 percent for the smooth surface; ±11 percent for the rough surfaces)

Downloaded 01 Apr 2008 to 131.122.81.5. Redistribution subject to ASME license or copyright; see http://www.asme.org/terms/Terms_Use.cfm

of this roughness was to tilt the large-scale structures towards the wall-normal direction, leading to a higher degree of isotropy and higher values of v'. This was not observed in the present results over the sandgrain roughness but was apparent in the flows over the algae-covered surfaces. The results of Schultz and Swain [9] indicated increases in both $\overline{u'^2}/U_\tau^2$ and $\overline{v'^2}/U_\tau^2$ for boundary layers over biofilms, although there was large degree of variability in their results.

Profiles of the turbulent shear stress, $\overline{-u'v'}/U_\tau^2$, for the test surfaces at $x=1.75$ m are shown in Fig. 11. The results of Ligrani and Moffat [12] for a fully-rough boundary layer on a uniform spheres rough surface are also included. Fairly good collapse of the smooth and sandgrain rough surfaces to single curve was observed. These profiles fell somewhat below the results of Ligrani and Moffat. This may have been due to Reynolds number effects. The results of Ligrani and Moffat are for a fully-rough boundary layer at $\mathrm{Re}_\theta=18{,}700$. The present values of Re_θ were significantly less ($\mathrm{Re}_\theta \leqslant 9{,}300$). It is interesting to note that Krogstad et al. [23] observed a moderate increase in the Reynolds shear stress for flows over a mesh *k*-type roughness. This was attributed to both an increase in the magnitude of the burst and sweep events and the frequency of these events. In the present study, a significant increase was observed in the Reynolds shear stress for the algae-covered surfaces in the log-law region. The increase was more variable for $\overline{-u'v'}/U_\tau^2$ than for $\overline{v'^2}/U_\tau^2$. Algae #1 had an increase of ~17 percent in $\overline{-u'v'}/U_\tau^2$ at 0.1δ as compared to the smooth and sandgrain rough walls. There was an increase of ~30 percent for algae #2 in the same region. A greater degree of scatter was seen in the algae profiles, and this can be attributed to the dynamic nature of the algae surface while under flow. It is of note that the peak in $\overline{-u'v'}/U_\tau^2$ corresponds approximately to the maximum extent of outward movement of the algae filaments.

In a recent study on a smooth wall and two rough walls (rods and mesh) with the same roughness function, Krogstad and Antonia [25] found that $\overline{u'^2}/U_\tau^2$ was largely unaffected by the nature of the surface except near the wall. However, they found significant differences in profiles of $\overline{v'^2}/U_\tau^2$ and $\overline{-u'v'}/U_\tau^2$ that extended well into the outer region of the boundary layer. It is interesting to note that the present algae results showed similar trends for all of these turbulence quantities.

Conclusion

Comparisons of turbulent boundary layers developing over filamentous marine algae with smooth and sandgrain rough surfaces have been made. A significant increase in C_f was measured for the algae-covered surfaces as compared with the smooth wall results. The increase averaged 125 percent and 110 percent for the two algae specimens tested. A significant increase was also noted in δ^*, θ, and δ for these surfaces. The present results show that the profiles of $\overline{u'^2}/U_\tau^2$, $\overline{v'^2}/U_\tau^2$, and $\overline{-u'v'}/U_\tau^2$ for boundary layers over the smooth and sandgrain rough walls collapse within experimental uncertainty. The algae-covered surfaces exhibited only a modest increase in $\overline{u'^2}/U_\tau^2$. More sizeable increase in $\overline{v'^2}/U_\tau^2$ and $\overline{-u'v'}/U_\tau^2$ were observed in the log-law region of the boundary layer. The region of increased $\overline{v'^2}/U_\tau^2$ extended well into the outer region (>2.5 times the maximum extent of outward movement of the algae filaments). The peak in the $\overline{-u'v'}/U_\tau^2$ profiles corresponded with the maximum extent of outward movement of the algae filaments. The present profiles of the turbulence quantities indicate that boundary layers over fairly uniform filamentous algae may become nearly self-similar. The roughness functions for these algae layers behave like *k*-type roughness, scaling to some degree on their mean height while under flow. Scatter in the roughness functions of these surfaces indicates that further research is needed to better correlate the physical measures of the algae layer with their roughness function.

Acknowledgments

I would like to thank the Division of Bioengineering and Environmental Systems at the National Science Foundation (grant BES9713110) and Prof. S. N. Gangadharan of Embry-Riddle Aeronautical University for supporting this research. Harbor Branch Foundation is also acknowledged for supporting the project with a postdoctoral fellowship for the author. Thanks go to B. Kovach at the Center for Corrosion and Biofouling Control at Florida Institute of Technology for measuring the surface profiles of the sandgrain rough surfaces. I also gratefully acknowledge Prof. P. Bradshaw, Prof. K. Flack, and Prof. C. Subramanian for reviewing drafts of this manuscript and providing many useful suggestions.

Nomenclature

B = log-law intercept
C_f = skin friction coefficient$=(\tau_0)/(1/2\rho U_e^2)$
E = elastic or Young's modulus
H = shape factor$=\delta^*/\theta$
I = moment of inertia of cross section of algae filament
k = roughness height
k_0 = undeflected roughness height
m = roughness density parameter
Re_θ = momentum thickness Reynolds number$=\theta U_e/\nu$
t = *t*-statistic
U, V = mean velocity in the *x* and *y* direction
U_e = freestream velocity
ΔU^+ = roughness function
u, v = instantaneous velocity in the *x* and *y* direction
u', v' = fluctuating velocity component in the *x* and *y* direction
U_τ = friction velocity$=\sqrt{\tau_0/\rho}$
x = streamwise distance from plate leading edge
y = normal distance from the boundary
α = statistical significance level
δ = boundary layer thickness
δ^* = displacement thickness
ε = wall datum error
κ = von Karman constant (=0.41)
ν = kinematic viscosity of the fluid
θ = momentum thickness
ρ = density of the fluid
τ_0 = wall shear stress

Superscript

$+$ = inner variable (normalized with U_τ or ν/U_τ)

References

[1] Callow, M. E., 1996, ''Ship Fouling: The Problem and Methods of Control,'' Biodeter. Abstracts, **10**, No. 4, pp. 411–421.
[2] Callow, M. E., 1986, ''Fouling Algae from 'In-Service' Ships,'' Botanica Marina, **24**, pp. 443–503.
[3] Schultz, M. P., 1998, ''The Effect of Biofilms on Turbulent Boundary Layer Structure,'' Florida Institute of Technology, Ph.D. Dissertation, May.
[4] Raupach, M. R., and Thom, A. S., 1981, ''Turbulence in and above Plant Canopies,'' Annu. Rev. Fluid Mech., **13**, pp. 97–129.
[5] Raupach, M. R., Antonia, R. A., and Rajagopalan, S., 1991, ''Rough-Wall Turbulent Boundary Layers,'' Appl. Mech. Rev., **44**, No. 1, pp. 1–25.
[6] Kouwen, N., and Unny, T. E., 1973, ''Flexible Roughness in Open Channels,'' ASCE J. Hydraul. Div., **99**, No. HY5, May, pp. 713–728.
[7] Lewkowicz, A. K., and Das, D. K., 1986, ''Turbulent Boundary Layers on Rough Surfaces With and Without a Pliable Overlayer: A Simulation of Marine Fouling,'' Int. Shipbuild. Prog., **33**, pp. 174–186.
[8] Ikeda, S., and Kanazawa, M., 1996, ''Three-Dimensional Organized Vortices above Water Plants,'' ASCE J. Hydrau. Eng., **122**, No. 11, pp. 625–633.
[9] Schultz, M. P., and Swain, G. W., 1999, ''The Effect of Biofilms on Turbulent Boundary Layers,'' ASME J. Fluids Eng., **121**, pp. 44–51.
[10] Gangadharan, S., Wimberly, C. R., Clark, A., and Collino, B., 1996, ''Design, Construction and Operation of a Cost Effective Water Tunnel at Harbor Branch Oceanographic Institution,'' Paper presented at SNAME Southeast Section Meeting, Oct. 11, Fort Pierce, FL.
[11] Klebanoff, P. S., and Diehl, F. W., 1951, ''Some Features of Artifically Thickened Fully Developed Turbulent Boundary Layers with Zero Pressure Gradient,'' NACA TN 2475.

Downloaded 01 Apr 2008 to 131.122.81.5. Redistribution subject to ASME license or copyright; see http://www.asme.org/terms/Terms_Use.cfm

[12] Ligrani, P. M., and Moffat, R. J., 1986, ''Structure of Transitionally Rough and Fully Rough Turbulent Boundary Layers,'' J. Fluid Mech., **162**, pp. 69–98.
[13] Perry, A. E., and Li, J. D., 1990, ''Experimental Support for the Attached-Eddy Hypothesis in Zero-Pressure Gradient Turbulent Boundary Layers,'' J. Fluid Mech., **218**, pp. 405–438.
[14] Coleman, H. W., and Steele, W. G., 1995, ''Engineering Application of Experimental Uncertainty Analysis,'' AIAA J., **33**, No. 10, pp. 1888–1896.
[15] Edwards, R. V., 1987, ''Report of the Special Panel on Statistical Particle Bias Problems in Laser Anemometry,'' ASME J. Fluids Eng., **109**, pp. 89–93.
[16] Buchhave, P., George, W. K., and Lumley, J. L., 1979, ''The Measurement of Turbulence with the Laser-Doppler Anemometer,'' Annu. Rev. Fluid Mech., **11**, pp. 443–503.
[17] Durst, F., Fischer, M., Jovanovic, J., and Kikura, H., 1998, ''Methods to Set Up and Investigate Low Reynolds Number, Fully Developed Turbulent Plane Channel Flows,'' ASME J. Fluids Eng., **120**, pp. 496–503.
[18] Coles, D., 1962, ''The Turbulent Boundary Layer in a Compressible Fluid,'' The Rand Corp., Rep. R-403-PR.
[19] Coles, D. 1969, ''The Young Person's Guide to the Data,'' Computation of Turbulent Boundary Layers–1968 AFOSR-IFP Stanford Conference, Vol. 2, D.E. Coles and E.A. Hirst, eds., Thermosciences Division, Stanford University, pp. 1–45.
[20] Colebrook, C. F., and White, C. M., 1937, ''Experiments with Fluid Motion in Roughened Pipes,'' Proc. R. Soc. London, Ser. A **161**, pp. 367–381.
[21] Schlichting, H., 1979, *Boundary-Layer Theory*, Seventh Edition, McGraw-Hill.
[22] Bandyopadhyay, P. R., 1987, ''Rough-Wall Turbulent Boundary Layers in the Transition Regime,'' J. Fluid Mech., **180**, pp. 231–266.
[23] Krogstad, P. A., Antonia, R. A., and Browne, L. W. B., 1992, ''Comparison Between Rough- and Smooth-Wall Turbulent Boundary Layers,'' J. Fluid Mech., **245**, pp. 599–617.
[24] Krogstad, P. A., and Antonia, R. A., 1994, ''Structure of Turbulent Boundary Layers on Smooth and Rough Walls,'' J. Fluid Mech., **277**, pp. 1–21.
[25] Krogstad, P. A., and Antonia, R. A., 1999, ''Surface Roughness Effects in Turbulent Boundary Layers,'' Exp. Fluids, **27**, pp. 450–460.

Downloaded 01 Apr 2008 to 131.122.81.5. Redistribution subject to ASME license or copyright; see http://www.asme.org/terms/Terms_Use.cfm